Computer Science Technical Report
TR-07-39
November 21, 2007

Emmanuel D. Blanchard, Adrian Sandu, and Corina Sandu

"A Polynomial Chaos Based Bayesian Approach for Estimating Uncertain Parameters of Mechanical Systems – Part II: Applications to Vehicle Systems"

Center for Vehicle Systems and Safety
Computer Science Department & Department of Mechanical Engineering
Virginia Polytechnic Institute and State University
Blacksburg, VA 24061
Phone: (540)-231-2193
Fax: (540)-231-9218
Email: sandu@cs.vt.edu
Web: http://www.eprints.cs.vt.edu

A Polynomial Chaos Based Bayesian Approach for Estimating Uncertain Parameters of Mechanical Systems - Part II: Applications to Vehicle Systems

Emmanuel D. Blanchard (eblancha@vt.edu)

Advanced Vehicle Dynamics Lab

Center for Vehicle Systems and Safety, Virginia Tech, Blacksburg, VA 24061– 0238

Adrian Sandu (sandu@cs.vt.edu)

Computer Science Department and the Center for Vehicle Systems and Safety

Virginia Tech, Blacksburg, VA 24061

Corina Sandu (csandu@vt.edu)

Advanced Vehicle Dynamics Lab

Center for Vehicle Systems and Safety, Virginia Tech, Blacksburg, VA 24061– 0238

ABSTRACT

This is the second part of a two-part article. In the first part, a new computational approach for parameter estimation was proposed based on the application of the polynomial chaos theory. The maximum likelihood estimates are obtained by minimizing a cost function derived from the Bayesian theorem. In this part, the new parameter estimation method is illustrated on a nonlinear four-degree-of-freedom roll plane model of a vehicle in which an uncertain mass with an uncertain position is added on the roll bar. The value of the mass and its position are estimated from periodic observations of the displacements and velocities across the suspensions. Appropriate excitations are needed in order to obtain accurate results. For some excitations, different combinations of uncertain parameters lead to essentially the same time responses, and no estimation method can work without additional information. Regularization techniques can still yield most likely values among the possible combinations of uncertain parameters resulting in the same time responses than the ones observed. When using appropriate excitations, the results obtained with this approach are close to the actual values of the parameters. The accuracy of the estimations has been shown to be sensitive to the number of terms used in the polynomial expressions and to the number of collocation points, and thus it may become computationally expensive when a very high accuracy of the results is desired. However, the noise level in the measurements affects the accuracy of the estimations as well. Therefore, it is usually not necessary to use a large number of terms in the polynomial expressions and a very large number of collocation points since the addition of extra precision eventually affects the results less than the effect of the measurement noise. Possible applications of this theory to the field of vehicle dynamics simulations include the estimation of mass, inertia properties, as well as other parameters of interest.

Keywords: Parameter Estimation, Polynomial Chaos, Collocation, Bayesian Estimation, Hammersley Algorithm, Halton Algorithm, Vehicle Dynamics

1. INTRODUCTION AND BACKGROUND

The polynomial chaos theory has been shown to be consistently more efficient than Monte Carlo simulations in order to assess uncertainties in mechanical systems [11, 12]. This paper extends the polynomial chaos theory to the problem of parameter estimation, and applies it to a four degree of freedom roll plane model of a vehicle with a mass added on the roll bar. Parameter estimation is an important problem, because many parameters simply cannot be measured physically with good accuracy, especially in real time applications. The method presented in this paper has the advantage of being able to deal with non-Gaussian parametric uncertainties.

Parameter estimation is a very difficult problem, especially for large systems, and a lot of effort devoted to it would be needed. Estimating a large number of parameters often proved to be computationally too expensive. This has led to the development of techniques determining which parameters affect the system's dynamics the most, in order to choose the parameters that are important to estimate [17]. Sohns, et al. [17] proposed the use of activity analysis as an alternative to sensitivity-based and principal component-based techniques. Their approach combines the advantages of the sensitivity-based techniques (i.e., being efficient for large models) and the sensitivity-based techniques (i.e., keeping parameters that can be physically interpreted). Zhang and Lu [22] combined the Karhunen–Loeve decomposition and perturbation methods with polynomial expansions in order to evaluate higher-order moments for saturated flow in randomly heterogeneous porous media.

The polynomial chaos method started to gain attraction after Ghanem and Spanos applied it successfully to the study of uncertainties in structural mechanics and vibration [4-7] using Wiener-Hermite polynomials. Xiu extended the approach to general formulations based on Wiener-Askey polynomials family [19], and applied it to fluid mechanics [18, 20, 21]. Authors applied for the first time the polynomial chaos method to multibody dynamic systems [11-14], terramechanics [10, 15], and parameter estimation [2, 3].

The fundamental idea of polynomial chaos approach is that random processes of interest can be approximated by sums of orthogonal polynomial chaoses of random independent variables. In this context, any uncertain parameter can be viewed as a second order random process (processes with finite variance; from a physical point of view they have finite energy). Thus, a second order random process viewed as a function of the random event θ, $(0 < \theta < 1)$, can be expanded in terms of orthogonal polynomial chaos [4], as detailed in Part I of this article: The Bayesian approach for parameter presentation explained in Part I of this article is applied to a roll plane modeling of a vehicle in the next section of this article.

2. APPLICATION TO A MORE COMPLEX MECHANICAL SYSTEM

2.1. Roll Plane Modeling of a Vehicle

The model used to apply the theory presented in this article is based on the four degree of freedom roll plane model of a vehicle used in [16] with the addition of a mass on the roll bar, which is shown in Figure 1. The difference is that the suspension dampers and the suspension springs used in this study are nonlinear and that a mass is added on the roll bar, which represents the driver, the passenger, and other objects in the vehicle. The added mass M and its position d_{CG} away from the left end of the roll bar are assumed to be uncertain. It is assumed that there is a passenger, and apriori distribution of the added mass will therefore be centered in the middle of the bar. This added mass will be represented as a point mass for the sake of simplicity. Measuring the position of the C.G. of the added mass physically is not straightforward. However, if a well defined road input can be used and sensors are available, these two parameters can be estimated based on the observed displacements and velocities across the suspensions.

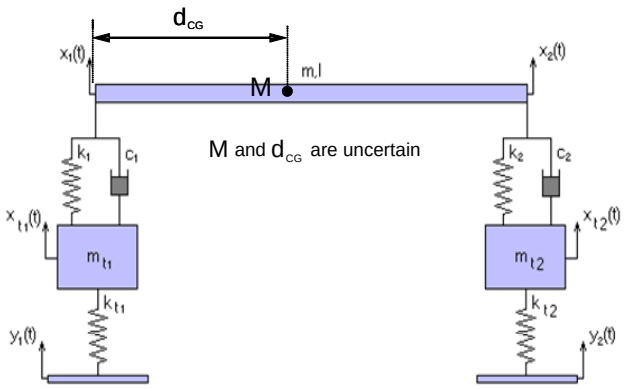

Figure 1. Four Degree of Freedom Roll Plane Model (adapted from [16]).

The body of the vehicle is represented as a bar of mass m (sprung mass) and length l that has a moment of inertia I. The unsprung masses, i.e., the masses of each tire/axle combination, are represented by m_{t1} and m_{t2}. A mass is added on the roll bar, which represents the driver and other objects in the vehicle. That added mass is represented as a point mass of value M situated at a distance d_{CG} from the left extremity of the roll bar.

The motion variables x_1 and x_2 correspond to the vertical position of each side of the vehicle body, while the motion variables x_{t1} and x_{t2} correspond to the position of the tires.

The inputs to this system are y_1 and y_2, which represent the road profile under each wheel.

If x is the relative displacement across the suspension spring with a stiffness k_i (i = 1, 2), the force across the suspension spring is given by:

$$F_{K_i}(x) = k_i x + k_{i,3}\, x^3, \quad i = 1, 2 \tag{1}$$

If v is the relative velocity across the damper with a damping coefficient c_i (i = 1, 2), the force across the damper is given by:

$$F_{C_i}(v) = c_i\left(0.2 \tanh(10v)\right) \tag{2}$$

For small angles, i.e. for $\dfrac{x_2 - x_1}{L}$ small, the equations of motion of the system are

$$\left(\frac{m+M}{2}\right)\left(\ddot{x}_2 + \ddot{x}_1 + (\ddot{x}_2 - \ddot{x}_1)\,\frac{M}{(m+M)}\,\left(2\,(d_{CG}/L) - 1\right)\right) + F_{K_1}(x_1 - x_{t1}) + F_{K_2}(x_2 - x_{t2}) + F_{C_1}(\dot{x}_1 - \dot{x}_{t1}) + F_{C_2}(\dot{x}_2 - \dot{x}_{t2}) = 0 \tag{3}$$

$$\cos\left(\left(\frac{x_2 - x_1}{L}\right) + \left(\frac{x_2 - x_1}{L}\right)_{STATIC}\right) \times \left[D\left(F_{K_1}(x_1 - x_{t1}) + F_{C_1}(\dot{x}_1 - \dot{x}_{t1})\right) - (L - D)\left(F_{K_2}(x_2 - x_{t2}) + F_{C_2}(\dot{x}_2 - \dot{x}_{t2})\right) + g\left(M(D - d_{CG}) - m\left(\frac{L}{2} - D\right)\right) \right]$$
$$+ \left(I + m\left(\frac{L}{2} - D\right)^2 + M\,(D - d_{CG})^2\right)\left(\frac{\ddot{x}_2 + \ddot{x}_1}{L}\right) = 0 \quad \textit{with} \quad D = \frac{M\, d_{CG} + m\,(L/2)}{M + m} \tag{4}$$

$$m_{t1}\ddot{x}_{t1} + F_{K_1}\left(x_{t1} - x_1\right) + F_{C_1}\left(\dot{x}_{t1} - \dot{x}_1\right) = k_{t1}\left(y_1 - x_{t1}\right) \tag{5}$$

$$m_{t2}\ddot{x}_{t2} + F_{K2}\left(x_{t2} - x_2\right) + F_{C_2}\left(\dot{x}_{t2} - \dot{x}_2\right) = k_{t2}\left(y_2 - x_{t2}\right) \tag{6}$$

where F_{K_1}, F_{K_2}, F_{C_1}, and F_{C_2} are defined in Equations (1) and (2).

In these equations, the variables are expressed versus their position at equilibrium (if the added mass *M* is not in the middle, we have static deflections). $\left(\frac{x_2 - x_1}{L}\right)_{STATIC}$ is relative to the position of the ground, which is fixed. It has to be estimated numerically because of the nonlinearities in the system.

The parameters used in this study are shown in Table 1. They are the parameters used by [16], with the addition of nonlinearities and uncertainties for M and d_{CG}. For the parameters shown in Table 1, the minimum static angle (i.e.., the angle of the roll bar with respect to a fixed reference on the ground) is -1.21 degrees and the maximum static angle is 1.21 degrees, which corresponds to $x_2 - x_1 = 0.032$ m. These values are obtained for $(\xi_1, \xi_2) = (1,1)$ and $(\xi_1, \xi_2) = (1,-1)$, i.e. for the maximum possible value of M with the added mass as far as possible from the center of the bar.

Table 1. Vehicle Parameters

Parameter	Description	Value
m	Mass of the Roll Bar	580 kg
m_{t1}, m_{t2}	Mass of the tire/axle	36.26 kg
c_1, c_2	Damping coefficients	710.70 N s /m
k_1, k_2	Spring constants – linear component	19,357.2 N/m
$k_{1,3}$, $k_{2,3}$	Spring constants – cubic component	100,000 N/m^3
l	Length of the Roll Bar	1.524 m
I	Inertia of the Roll Bar	63.3316 kg m^2
k_{t1}, k_{t2}	Tires vertical stiffnesses	96,319.76 N/m
M	Added Mass	200 kg +/-50%, with Beta (1, 1) distribution
d_{CG}	Distance between the C.G. of the mass and the left extremity of the roll bar	0.7620 m +/-25%, with Beta (1, 1) distribution

The uncertainties of 50% and 40% on the values of M and d_{CG} can be represented as:

$$M = M_{nom}(1 + 0.50\,\xi_1), \quad \xi_1 \in [-1,\ 1] \tag{7}$$

$$d_{CG} = d_{CG,nom}(1 + 0.25\,\xi_2), \quad \xi_2 \in [-1,\ 1] \tag{8}$$

where M_{nom} and $d_{CG,\,nom}$ are the nominal values of the vertical stiffnesses of the tires ($M_{nom} = 200$ kg and $d_{CG,\,nom} = 0.7620$ m).

It is assumed that the probability density functions of the values of M and d_{CG} can be represented with Beta (1, 1) distributions, with uncertainties of +/- 50% and +/- 25%, respectively. The distributions of the uncertainties related to the values of M and d_{CG}, defined on the interval $[-1, 1]$, are represented in Figure 2. They have the following Probability Density Functions (PDFs):

$$w(\xi_i) = \frac{3}{4}\left(1-\xi_i^{\,2}\right), \quad i = 1, 2 \tag{9}$$

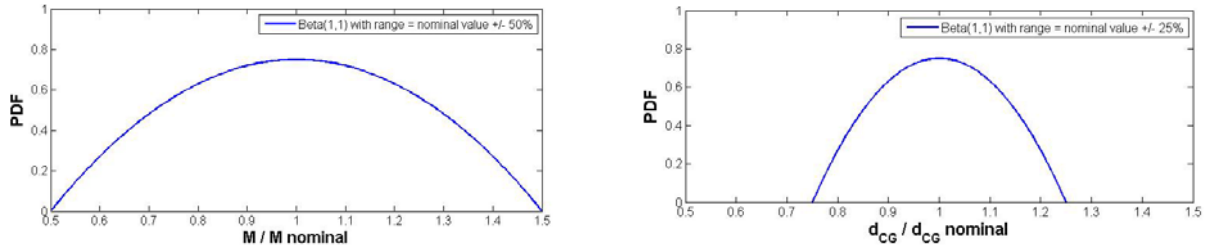

(a) (b)

Figure 2. Beta (1, 1) Distribution; (a) for Value of the Mass, (b) for Value of the Position of the C.G. of the Mass

2.2. Collocation Points

The generalized polynomial chaos theory is explained in [11] in which direct stochastic collocation is proposed as a less expensive alternative to the traditional Galerkin approach. The collocation approach consists of imposing that the equation system holds at a given set of collocation points. If the polynomial chaos expansions contain 15 terms for instance, then at least 15 collocation points are needed in order to have at least 15 equations for 15 unknown polynomial chaos coefficients. It is desirable to have more collocation points than polynomial coefficients to solve for. In that case a least-squares algorithm is used to solve the system with more equations than unknowns.

Unless otherwise specified, the polynomial chaos expansions of M and d_{CG} will use 15 terms. All the other variables affected by the uncertainties on M and d_{CG} will be modeled by a polynomial chaos expansion using 15 terms as well. The collocation approach is the one used in this study. It requires at least 15 collocation points to derive the coefficients associated to each of the 15 terms of the different polynomial chaos expansions.

Unless otherwise specified, 30 collocation points will be used to derive the coefficients associated to each of the 15 terms of the different polynomial chaos expansions. The collocation points used in this study are obtained using an algorithm based on the Halton algorithm [8], which is similar to the Hammersley algorithm [9]. These collocation points for a uniform distribution are shown in Figure 3 (a).

One of the advantages of the Hammersley/Halton points used in this study is that when the number of points is increased, the new set of points still contains all the old points. We therefore know that more points should result in a better approximation. The collocation points for a Beta (1, 1) distribution, which is used in this study, are shown in Figure 3 (b).

The transformation from the collocation points for a uniform distribution to the points for a Beta (1, 1) distribution is achieved by applying the inverse Cumulative Distribution Function of the Beta (1, 1) distribution. Let's note that there is no collocation point at the boundary, i.e., no point associated with an uncertainty equal to -1 or 1, which is needed in order to avoid having a cost function equal to infinity.

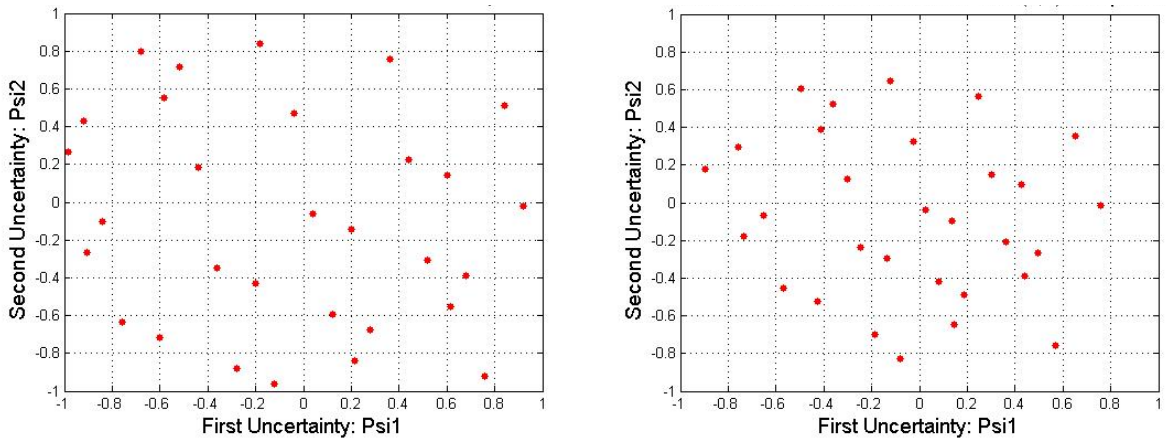

Figure 3. Halton Collocation Points (2-Dimensions, 30 Points: (a) for Uniform Distribution; (b) for Beta (1, 1) Distribution

2.3. Experimental Setting – Road Input

In order to assess the efficiency of the polynomial chaos theory for parameter estimation, M and d_{CG} will be estimated using observations of four motion variables obtained for a given road input: the displacements across the suspensions ($x_1 - x_{t1}$ and $x_2 - x_{t2}$), and their corresponding velocities ($\dot{x}_1 - \dot{x}_{t1}$ and $\dot{x}_2 - \dot{x}_{t2}$). The road profile is shown in Figure 4, and the road input is obtained assuming the vehicle has a constant speed of 16 km/h (10 mph). The road profile can be seen as a long speed bump. The first tire is subjected to a ramp at t = 0, and reaches a height of 10 cm (4") for a horizontal displacement of 1m, then stays at the same height for 1m, and goes back down to its initial height. The second tire is subjected to the same kind of input, but with a time delay of 20% and it reaches a maximum height of only 8 cm.

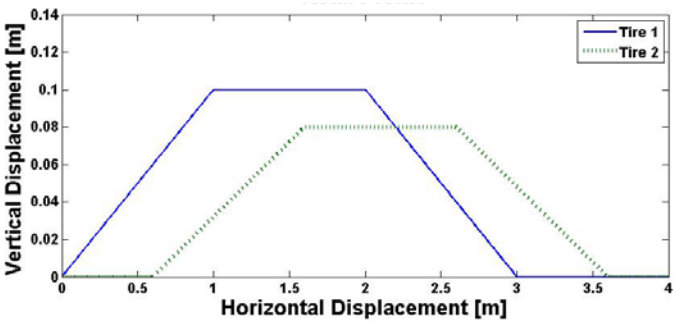

Figure 4. Road Profile

The four motion variables are plotted from $t = 0$ to $t = 3\,\text{seconds}$ using $M^{ref} = 223.26\ \text{kg}$ and $d_{CG}{}^{ref} = 0.6882\,\text{m}$ (i.e., $\xi_1{}^{ref} = 0.2326$ and $\xi_2{}^{ref} = -0.3875$) and assuming these values can only be measured with a sampling rate of $0.3\,\text{s}$.

However, for the proof of concept of the parameter estimation method presented in this paper, we pretend we do not know the values of M and d_{CG}, the objective being to estimate those values based on the plot of the four motion variables shown in Figure 5. Let's note that 3 seconds of data correspond to a horizontal displacement of 13.33 meters. The end of the speed bump occurs at $t = 0.675\,\text{s}$.

The excitation signal is supposed to be perfectly known. In other words, the road profile shown in Figure 4 is supposed to be exactly known and the speed of the vehicle is supposed to be exactly 16 km/h at all time, which enables us to use any desired sampling rate for the input signal. However, only 10 measurement points are used for the output

displacements and velocities (not counting the measurements at t = 0, which give no useful information in order to estimate the unknown parameter). It is always better to take a number of measurement points as large as possible when computational time is not an issue and precision is very important. However, using a lower number of measurements can be useful when an answer is needed quickly, which does not prevent from continuing to process the extra information later on if needed, knowing that the extra measurements will generally yields more precision. Adding more measurement points does not usually add much precision to the estimations, as will be shown later in this article.

As explained in the first part of this article, the quality of the maximum likelihood estimate is related to the shape of the Bayesian cost function, with a sharp minimum indicating an accurate estimate. Inaccurate estimates can be caused by different factors, including a sampling rate below the Nyquist frequency, non-identifiability, non-observability, and an excitation signal that is not rich enough.

The parameters are non-identifiable when different parameter values lead to identical system outputs. In this case the Bayesian cost function has an entire region of minima (e.g., a valley), with each parameter value in the region being equally likely. A regularization approach based on increasing the weight of the apriori information can be used to select reasonable estimates.

For identifiable and observable systems accurate estimates can be obtained in most cases even if the output signal is sampled below the Nyquist rate. In the worst case, however, sampling below the Nyquist rate cannot guarantee that sufficient information is extracted from the output. In this worst case the apriori information becomes important and the estimate is biased toward the apriori most likely value.

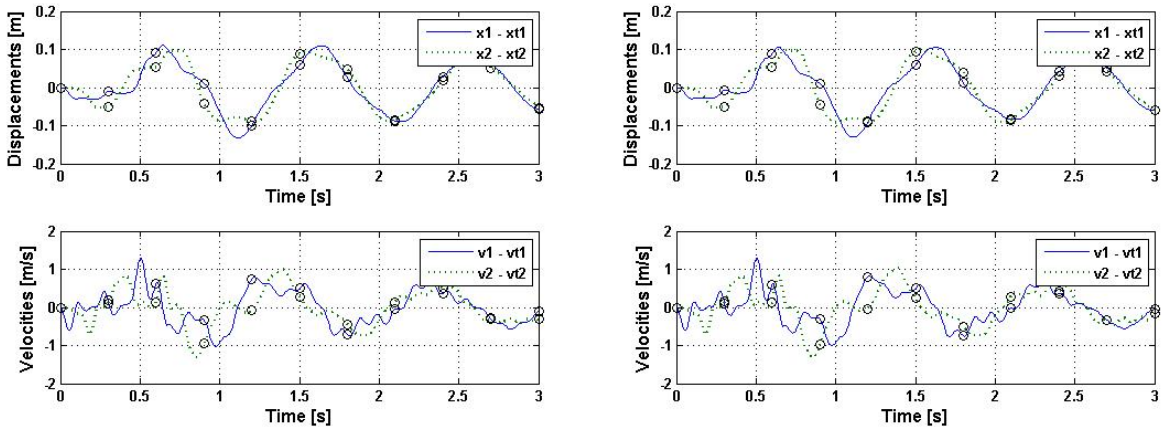

(a) (b)

Figure 5. Observed States - Displacements and Velocities: (a) Measured; (b) For Nominal Values ($\xi_1 = 0$, $\xi_2 = 0$)

The measurements shown in Figure 5 (a) are synthetic measurements obtained from a reference simulation with the reference value of the uncertain parameter $\xi_1^{ref} = 0.2326$ and $\xi_2^{ref} = -0.3875$. Parameters estimation is performed using the Bayesian approach. In order to work with a realistic set of measurements, a Gaussian measurement noise with zero mean and 1% variance is added to the observations shown in Figure 5 (for the relative displacements and velocities) before performing parameter estimation.

The state of the system at future times depends on the random initial velocity and can be represented by

$$y(\xi,t) = \left[x_1(\xi,t) \quad x_2(\xi,t) \quad x_{t1}(\xi,t) \quad x_{t2}(\xi,t) \quad \frac{dx_1(\xi,t)}{dt} \quad \frac{dx_2(\xi,t)}{dt} \quad \frac{dx_{t1}(\xi,t)}{dt} \quad \frac{dx_{t2}(\xi,t)}{dt} \quad \theta(\xi,t) \right]^T \tag{10}$$

If we assume that only the displacements across the suspensions ($x_1 - x_{t1}$ and $x_2 - x_{t2}$), and their corresponding velocities ($\dot{x}_1 - \dot{x}_{t1}$ and $\dot{x}_2 - \dot{x}_{t2}$) can be measured, then

$$H = \begin{bmatrix} 1 & 0 & -1 & 0 & 0 & 0 & 0 & 0 & 0 \\ 0 & 0 & 0 & 0 & 1 & 0 & -1 & 0 & 0 \\ 0 & 1 & 0 & -1 & 0 & 0 & 0 & 0 & 0 \\ 0 & 0 & 0 & 0 & 0 & 1 & 0 & -1 & 0 \end{bmatrix} \tag{11}$$

and the measurements yield

$$z_k = H \cdot y^{\text{ref}}(t_k) + \varepsilon_k = x^{\text{ref}}(t_k) + \varepsilon_k, \quad \varepsilon_k \in \mathrm{N}(0, R_k). \tag{12}$$

Measurement errors at different times are independent random variables. The measurement noise ε_k is assumed to be Gaussian with a zero mean and a variance 1% (or 0.01% when indicated) of the value of $x(t)$. The diagonal elements of the covariance matrix of the uncertainty associated with the measurements will still be set to at least 10^{-12} when necessary so that R_k^{-1} can always be computed. Therefore, the covariance of the uncertainty associated with the measurements is

$$R_k = \begin{bmatrix} R_{k1} & 0 & 0 & 0 \\ 0 & R_{k2} & 0 & 0 \\ 0 & 0 & R_{k3} & 0 \\ 0 & 0 & 0 & R_{k4} \end{bmatrix} \tag{13}$$

where

$$R_{k1} = \max\left\{10^{-12}, (0.01\ z_{k1})^2\right\} \tag{14}$$

$$R_{k2} = \max\left\{10^{-12}, (0.01\ z_{k2})^2\right\} \tag{15}$$

$$R_{k3} = \max\left\{10^{-12}, (0.01\ z_{k3})^2\right\} \tag{16}$$

$$R_{k4} = \max\left\{10^{-12}, (0.01\ z_{k4})^2\right\} \tag{17}$$

As explained in the first part of this article, the maximum likelihood estimate is obtained by minimizing the Bayesian cost function

$$J_{\text{total}}(\xi) = \underbrace{\tfrac{1}{2}\sum_{k=1}^{N}\left(z_k - Hy(\xi, t_k)\right)^T R_k^{-1}\left(z_k - Hy(\xi, t_k)\right)}_{J_{\text{mismatch}}} + \underbrace{\left(-\log\left(\rho(\xi)\right)\right)}_{J_{\text{apriori}}} \tag{18}$$

For this particular example, the joint probability density function $\rho(\xi)$ is

$$\rho(\xi) = \frac{3}{4}\left(1 - \xi_i^{\,2}\right) \times \frac{3}{4}\left(1 - \xi_2^{\,2}\right) \tag{19}$$

The value of the cost function can be visualized, as shown in Figure 6. A simple Matlab code can estimate the values of ξ_1 and ξ_2 (and thus the values of M and d_{CG}) corresponding to the minimum value of the cost function.

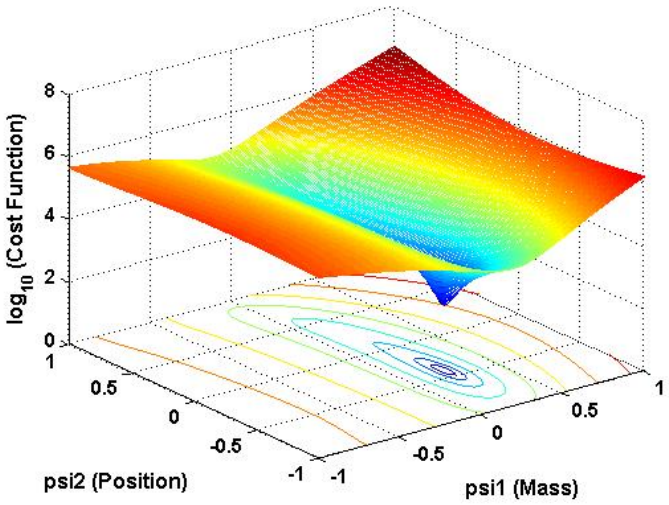

Figure 6. Cost Function Using the Bayesian Approach – 10 time points (Noise = 1%)

The estimated values of ξ_1 and ξ_2 obtained using the Bayesian approach are $\xi_1^{\,est} = 0.2236$ and $\xi_2^{\,est} = -0.4024$, i.e., $M^{\,est}$ 222.36 kg and $d_{CG}^{\,est} = 0.6853$ m. The actual values were $\xi_1^{\,ref} = 0.2326$ and $\xi_2^{\,ref} = -0.3875$, i.e., $M^{\,ref} = 223.26$ kg and $d_{CG}^{\,ref} = 0.6882$ m. It seems to be a good estimation since there is noise associated to the measurements. With a Gaussian measurement noise with zero mean and 0.01% variance the results would be $\xi_1^{\,est} = 0.2237$ and $\xi_2^{\,est} = -0.3992$, i.e., $M^{\,est} = 222.37$ kg and $d_{CG}^{\,est} = 0.6860$ m. It shows that the effects of a Gaussian measurement noise with zero mean and 1% variance cannot be completely neglected.

Figure 7 shows the cost function that would be obtained if the motion variables could be measured with a sampling rate of 0.03 s, for a noise level of 1%. It can be observed that the extra measurement point do not change the shape of the cost function by much. The fact that the cost function had a well defined minimum value with 10 measurement points told us that we had enough information in order to obtain a precise estimation that can be trusted. Using 100 measurement points will add more accuracy, but not so much considering the computing time will be 10 times greater.

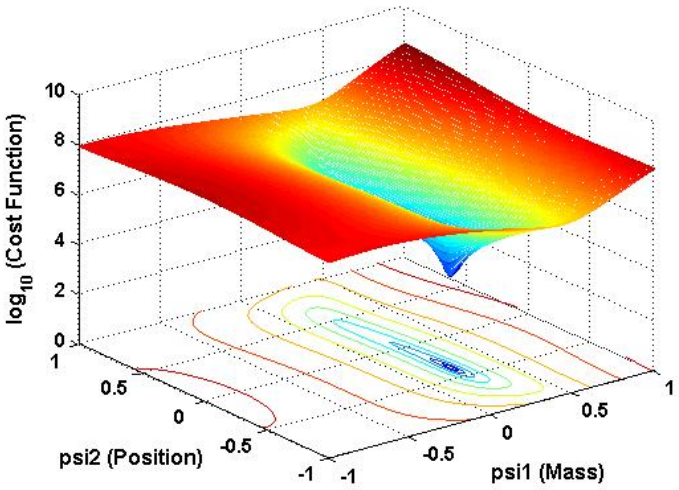

Figure 7. Cost Function Using the Bayesian Approach – 100 time points (Noise = 1%)

With 100 sample points and a noise level of 1%, which corresponds to the cost function shown in Figure 7, the estimated values of ξ_1 and ξ_2 obtained using the Bayesian approach are $\xi_1^{est} = 0.2339$ and $\xi_2^{est} = -0.3662$, i.e., $M^{est} = 223.39$ kg and $d_{CG}^{est} = 0.6922$ m. The estimation of ξ_1 (i.e., of the added mass) is more accurate than 10 measurement points, but the estimation of ξ_2 is not more accurate in this case. With a Gaussian measurement noise of 0.01% variance, the results would be $\xi_1^{est} = 0.2341$ and $\xi_2^{est} = -0.3736$, i.e., $M^{est} = 223.41$ kg and $d_{CG}^{est} = 0.6908$ m, which also yields a more accurate estimation of the added mass when compared with the results obtained with 10 measurement points. As a conclusion, adding more measurements points adds accuracy. However, the shape of the cost function indicated that the estimation using only 10 measurement points was already quite accurate. Adding more measurement points is not the only thing that affects the results. Table 2 shows that the results of the estimation process are also affected by the number of terms used in the polynomial chaos approximation and by the number of collocation points. Adding more measurement point is desirable if the computational cost is not already high, which also depends on the complexity of the system. If the computational time is an issue and the cost function yields a clear minimum, not adding more measurements might be a good idea then.

Table 2. Effect of the Polynomial Chaos Approximation for the Bayesian Approach (with 10 time points and a Gaussian measurement noise with zero mean and 1% variance)

Number of Collocation Points	10 terms	15 terms	21 terms
10	0.2305, -0.3864		
15	0.2249, -0.3793	0.2307, -0.3790	
21	0.2218, -0.3918	0.2307, -0.3885	0.2239, -0.5036
30	0.2224, -0.3869	**0.2236, -0.4024**	0.2279, -0.4012
40			0.2275, -0.4004
45		0.2257, -0.4006	
60			0.2270, -0.3972
Actual Values	**0.2326, -0.3875**	**0.2326, -0.3875**	**0.2326, -0.3875**

Table 2 shows that the estimations obtained with 15 terms become similar to the observations obtained with 21 terms as the number of collocation points gets larger. Therefore, working with 15 terns in the polynomial chaos expansions and with 30 collocation points seems to be a good comprise. Adding more terms and more collocation points would increase the precision of the estimation, but the extra precision would eventually become small compared with the effect of the noise, and would come at a great computational cost.

It can be noticed that when using the minimum number of collocation points required to perform the estimation, i.e., a number of collocation points equal to the number of terms, increasing the number of terms results in poorer estimations. This is something that has been observed on other test cases. For this case, it becomes very noticeable when using 21 terms and 21 collocation points. This makes sense since solving a system with more unknowns is more complicated, and adding extra information into a least squares algorithm becomes more valuable as the system becomes more complex.

The fact that the estimation performed with 10 collocations for 10 terms seems to be due to a very favorable random choice of the collocation points. Using 10 terms in the polynomial chaos expressions results in approximations. Using only 10 collocation points also results in less precision. However, many approximations can still lead to an accurate result when they cancel out each other by chance.

2.4. Results for a Chirp Input

In this section, linear swept-frequency sine input signals are used from $t = 0$ to $t = 3\,\text{seconds}$ with frequencies ranging from 0 Hz at $t = 0$ to 2 Hz at $t = 3\,\text{seconds}$, as shown as in Figure 8. The amplitude of the input signals is 5 cm. The reason why the highest frequency of the chirp input used in this study is 2 Hz is that it is when the dampers start being in saturation mode for a very significant percentage of the time due to higher velocities, which will be shown later. When the dampers saturate, there is no one-to-one relationship between the relative velocities across the dampers and the fore they produce, which can leads to non-identifiability.

The inputs signals are:

$$y_1 = 0.05\ \sin\left(t\frac{2\pi}{3}t\right), \quad i.e.\ \ y_1 = 0.05\ \sin\left(\omega(t)\times t\right)\ \text{with}\ \ \omega(t) = \frac{2\pi}{3}t \tag{20}$$

$$y_2 = -0.05\ \sin\left(t\frac{2\pi}{3}t\right), \quad i.e.\ \ y_2 = -0.05\ \sin\left(\omega(t)\times t\right)\ \text{with}\ \ \omega(t) = \frac{2\pi}{3}t \tag{21}$$

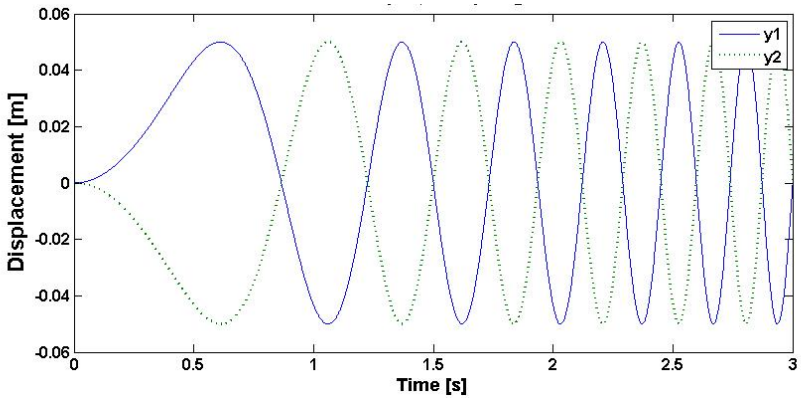

Figure 8. Chirp Input going from DC to 2 Hz in 3 seconds

Parameters estimation is performed using the Bayesian approach. In order to work with a realistic set of measurements, a Gaussian measurement noise with zero mean and 1% variance is added to the observed relative displacements and velocities before performing parameter estimation. Figure 9 shows the cost function obtained with a sampling rate of 0.1 s, for a noise level of 1%. Since the maximum frequency in the chirp input is 2 Hz, using 30 measurement points is enough in order to respect the Nyquist criterion.

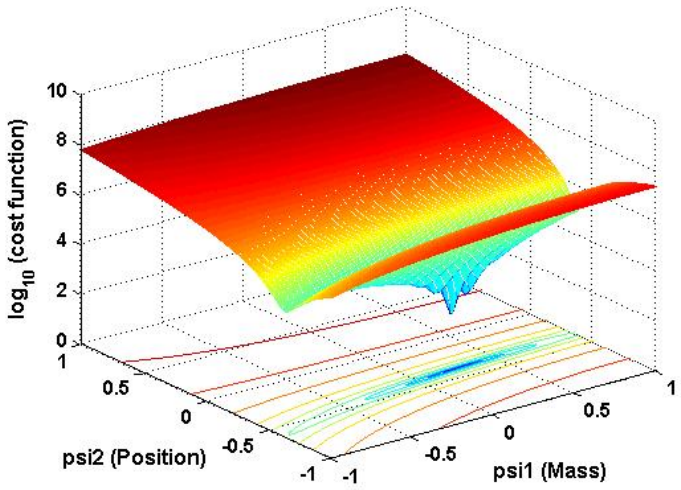

Figure 9. Cost Function for the Chirp Input with 30 Time Points and 1% Measurement Noise

The estimated values of ξ_1 and ξ_2 obtained using the Bayesian approach are $\xi_1^{\,est} = 0.2381$ and $\xi_2^{\,est} = -0.3868$, i.e., $M^{\,est}$ 223.81 kg and $d_{CG}^{\,est} = 0.6883$ m. The actual values were $\xi_1^{\,ref} = 0.2326$ and $\xi_2^{\,ref} = -0.3875$, i.e., $M^{\,ref} = 223.26$ kg and $d_{CG}^{\,ref} = 0.6882$ m. Using a chirp signal is therefore a good way to estimate the value of the mass and its position, as long as it doesn't contain frequencies where the dampers are in saturation mode most of the time. The cost function has a clear minima, but it can be seen that this minima is in a region of low values along the line. Adding higher frequency content in the input signal would start preventing us from obtaining a clear minima along this line. This is illustrated in the next section.

2.5. Relationship Between Quality of Estimation and the Frequency of the Input Signal

In order to assess the efficiency of the polynomial chaos theory for parameter estimation, M and d_{CG} will be estimated using a plot of four motion variables: the displacements across the suspensions ($x_1 - x_{t1}$ and $x_2 - x_{t2}$), and their corresponding velocities ($\dot{x}_1 - \dot{x}_{t1}$ and $\dot{x}_2 - \dot{x}_{t2}$). The estimations will be performed for different harmonic inputs, ranging from 0.33 Hz to 25 Hz, with amplitudes of +/- 0.05 m for y_1 and y_2. The input signals are still supposed to be rich enough, i.e., they are supposed to be exactly known, which enables us to use any desired sampling rate for the input signal. Figure 10 shows the harmonic inputs that will be used at 1 Hz.

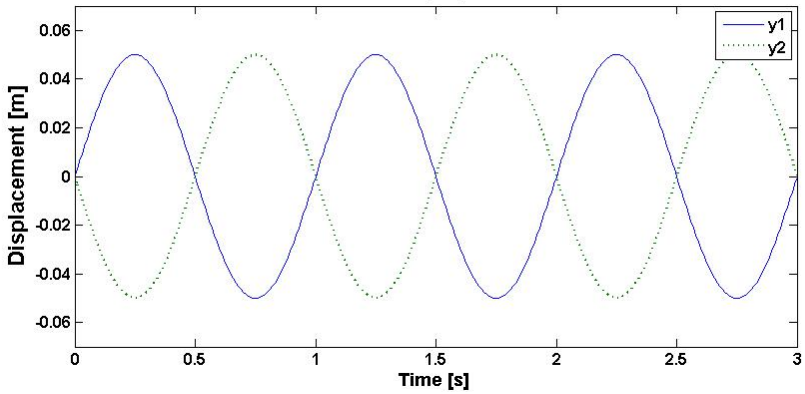

Figure 10. Road Input at 1 Hz

The estimations are performed using 15 terns in the polynomial chaos expansions and 30 collocation points. Figure 11 shows the estimated values of M and d_{CG}, obtained using the Bayesian approach for harmonic inputs with frequencies ranging from 0.33 Hz to 25 Hz. It is still assumed that measurements can only be obtained at a sampling rate of 0.3 s and that the Gaussian measurement noise has a zero mean and 1% variance. It can be observed that good estimation are obtained for frequencies lower than or equal to 1.33 Hz, but the quality of the estimations is clearly poorer for frequencies higher than or equal to 1.66 Hz.

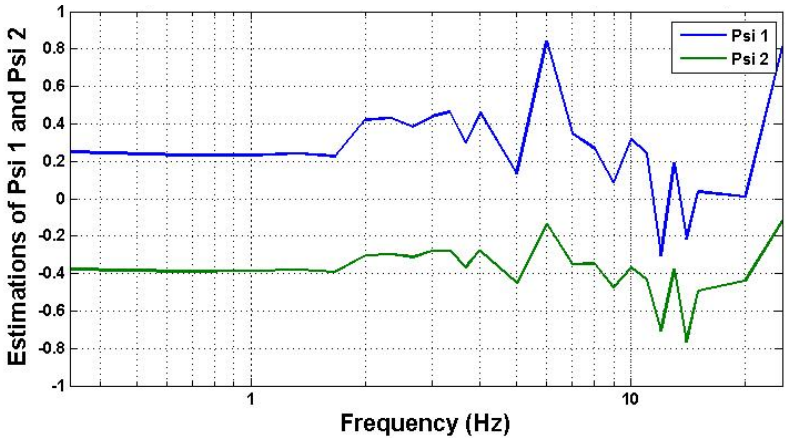

Figure 11. Bayesian Estimation of the Added Mass and the Position of the Mass at Different Frequencies Using 10 Time Points and a 1% Noise

One might wonder if increasing the sampling rate of the measurement and being able to work with an extremely low measurement noise level would improve the results. Figure 12 shows the estimated values of M and d_{CG} obtained with a sampling rate of 0.3 s (i.e., 10 time points) for the Bayesian approach when the Gaussian measurement noise has a 0.01% variance instead of a 1%. It can be observed that even though the estimations can be different, the same problems remain for estimating M (i.e. ξ_1) at frequencies higher than or equal to 2 Hz estimated values of However, the estimation of d_{CG} (i.e. ξ_2) yields much better results at frequencies higher than or equal to 2 Hz.

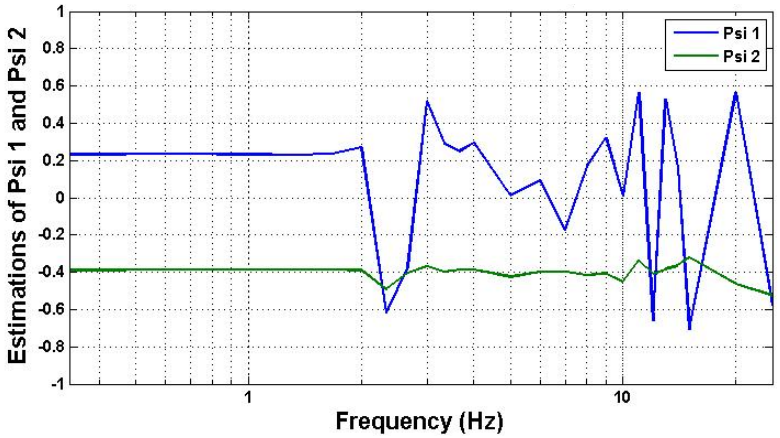

Figure 12. Bayesian Estimation of the Added Mass and the Position of the Mass at Different Frequencies Using 10 Time Points and a 0.01% Noise

One might wonder if being able to increase the sampling rate of the measurement instead of being able to work with an extremely low measurement noise level would improve the results. Figure 13 shows the estimated values of M and d_{CG} obtained with a sampling rate of 0.02 s (i.e., 150 time points) for the Bayesian approach when the Gaussian measurement noise has a 1% variance. It can be observed that the results are very similar than the results obtained with 10 time points and a 0.01% noise. Being able to increase the sampling rate and being to lower the noise level both have the same effect on the quality of the estimations. The same problems remain for estimating M (i.e. ξ_1) at frequencies higher than or equal to 2 Hz

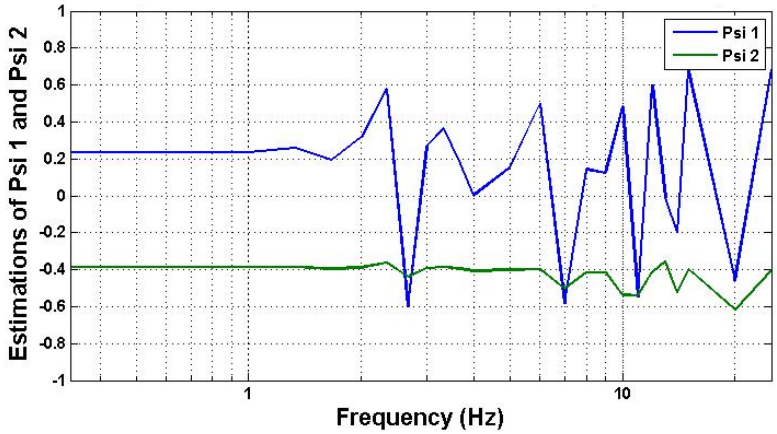

Figure 13. Bayesian Estimation of the Added Mass and the Position of the Mass at Different Frequencies Using 150 Time Points and a 1% Noise

One might wonder if increasing the sampling rate of the measurement while still being able to work with an extremely low measurement noise level would improve the results. Figure 14 shows the estimated values of M and d_{CG} obtained with a sampling rate of 0.02 s (i.e., 150 time points) for the Bayesian approach when the Gaussian measurement noise has a 0.01%. It can be observed that even though the estimations can be different, the same problem remains for frequencies higher than or equal to 2 Hz. It can be observed that the results are still very similar than for the previous two configurations and that the same problems remain for estimating M (i.e. ξ_1) at frequencies higher than or equal to 2 Hz. When the noise level is extremely low, adding extra measurement points does not yield better results.

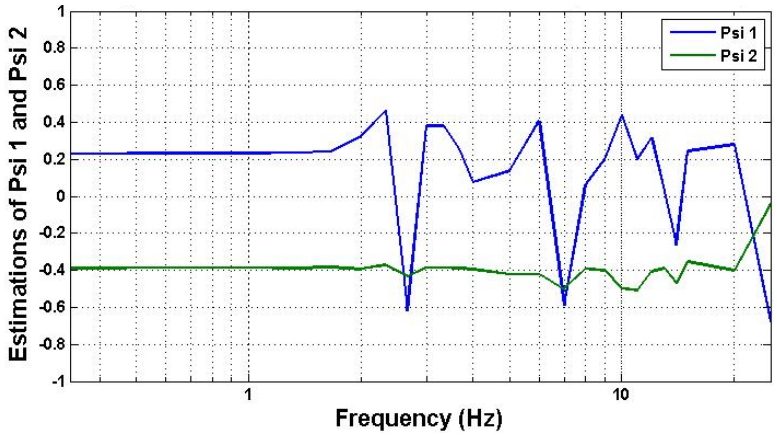

Figure 14. Bayesian Estimation of the Added Mass and the Position of the Mass at Different Frequencies Using 150 Time Points and a 0.01% Noise

Therefore, the mass cannot be estimated when using inputs at frequency higher than or equal to 2 Hz even with measurements of very good quality. The reason the estimations are not accurate for input frequencies of 2 Hz and above is a problem of non-identifiability: different values of M and d_{CG} can result in the same time response for the displacements and velocities across the suspensions. For instance, if we look at the cost function at 1 Hz with 10 time points and a 0.01% measurement noise added to the observations, as shown in Figure 15, we can see that the cost function has a clear minimum. If we look at the cost function at 2 Hz, as shown in Figure 16, we can see that the cost function has minima along a curve. Those minima correspond to several combinations (M, d_{CG}) yielding the same time response for the 2 Hz input. The estimated values ($\xi_1^{\,est} = 0.2707$ and $\xi_2^{\,est} = -0.3890$) and the actual values ($\xi_1^{\,ref} = 0.2326$ and $\xi_2^{\,ref} = -0.3875$) are both on this curve containing the minima. Figure 17 shows he cost function at 3 Hz, which yields no clear minimum as well.

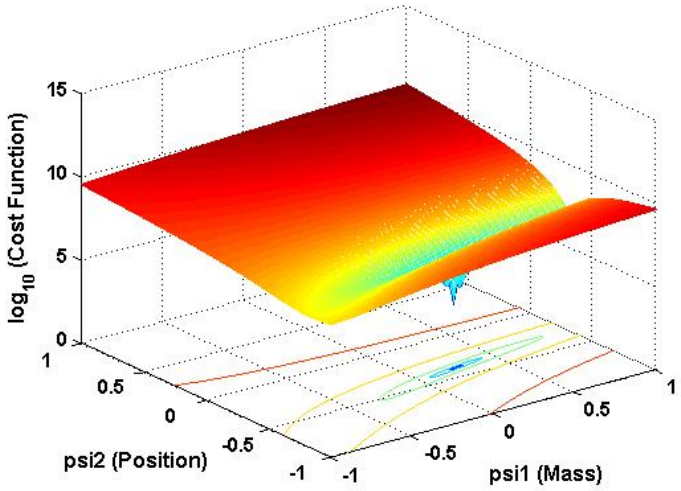

Figure 15. Cost Function at 1 Hz with 10 Time Points and 0.01% Measurement Noise

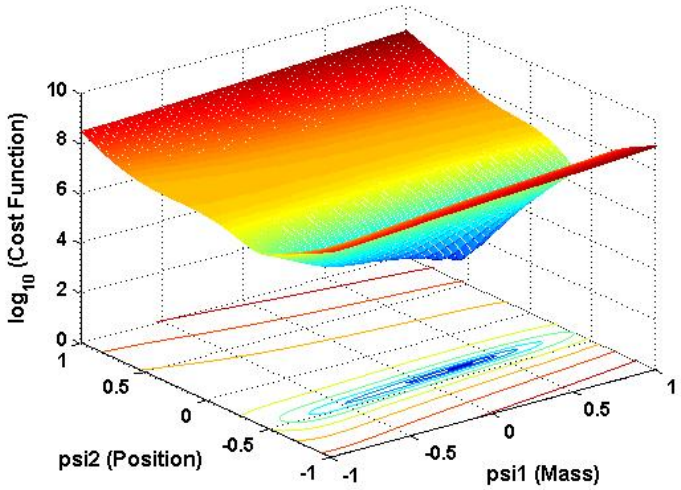

Figure 16. Cost Function at 2 Hz with 10 Time Points and 0.01% Measurement Noise

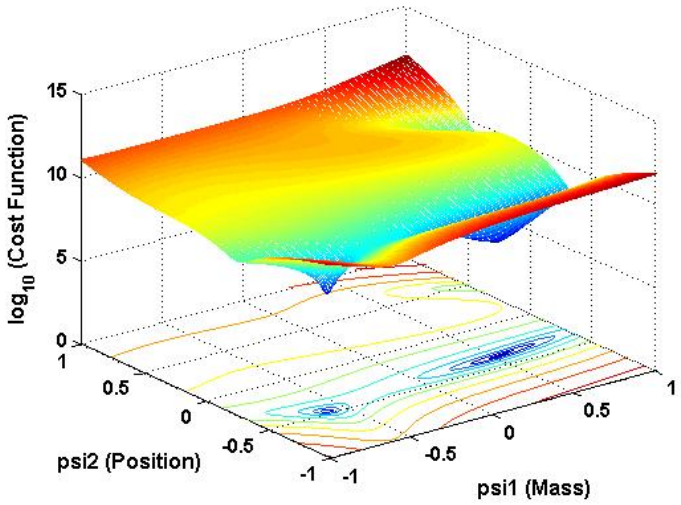

Figure 17. Cost Function at 3 Hz with 10 Time Points and 0.01% Measurement Noise

Figure 18 shows the time responses at 1 Hz for the nominal values $(\xi_1, \xi_2) = (0, 0)$ and for values that were used $(\xi_1, \xi_2) = (0.2326, -0.3875)$, which were estimated very well by the Bayesian approach . It can be noticed that the curves are quite distinct.

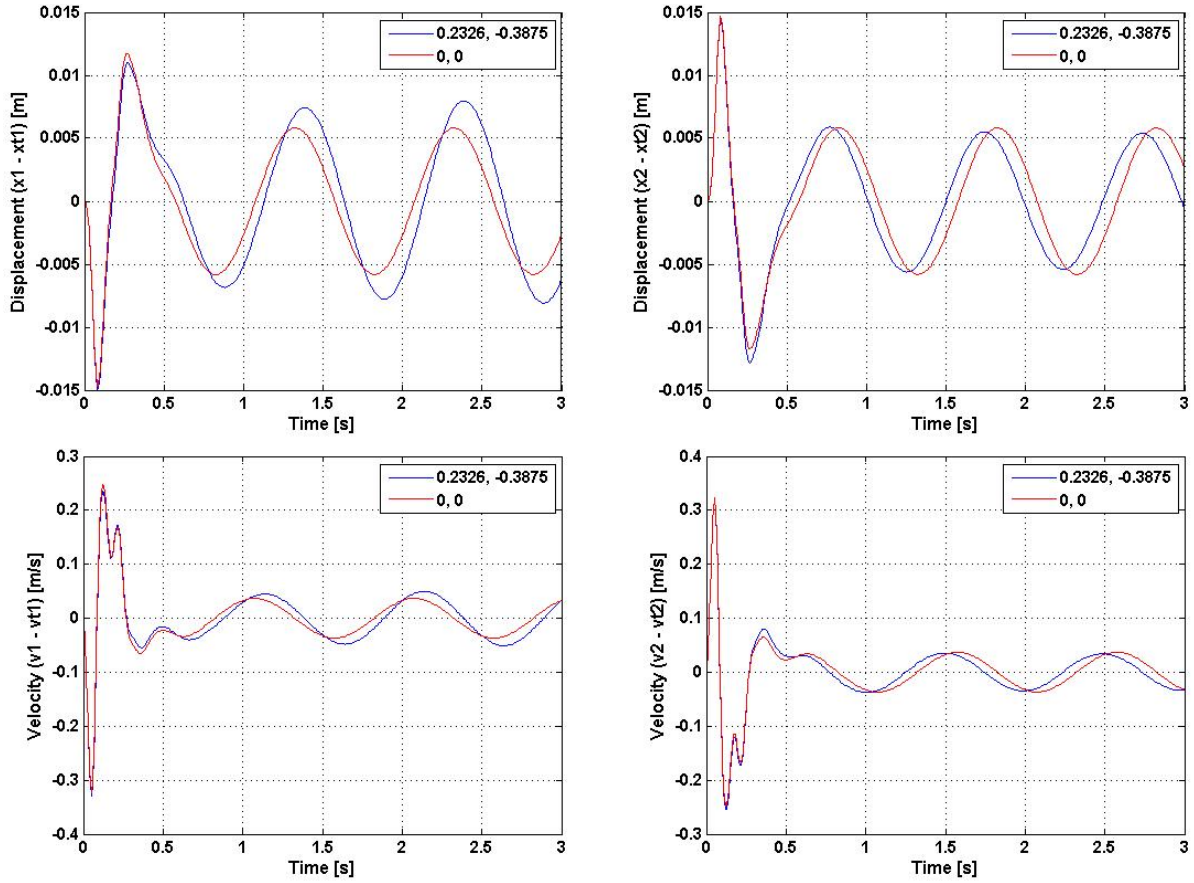

Figure 18. Time Responses at 1 Hz

Figure 19 shows the time responses at 2 Hz for the nominal values $(\xi_1, \xi_2) = (0, 0)$, for the values that were used $(\xi_1, \xi_2) = (0.2326, -0.3875)$, for the estimated values $(\xi_1, \xi_2) = (0.2707, -0.3890)$. It shows that the estimated values yield the same time response than the actual values at 2Hz, which is why no estimation technique can work. Also, the observed time response is more similar to the nominal time response than it was at 1 Hz, which is why estimating uncertainties gets more difficult in a more general sense.

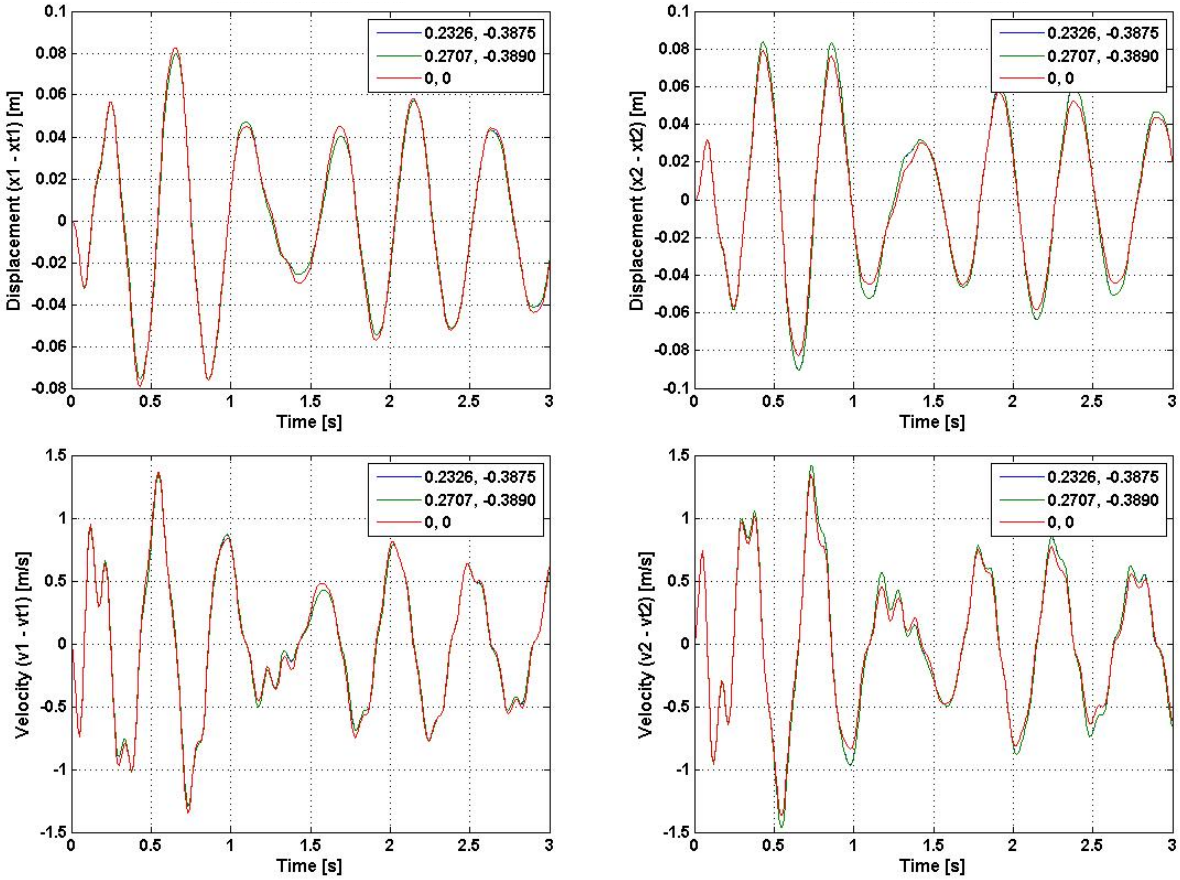

Figure 19. Time Responses at 2 Hz

Figure 20 shows the time responses at 3 Hz for the nominal values $(\xi_1, \xi_2) = (0, 0)$, for the values that were used $(\xi_1, \xi_2) = (0.2326, -0.3875)$, for the values that were used $(\xi_1, \xi_2) = (0.5188, -0.3690)$. It shows that the estimated values yield the same time response than the actual values at 3Hz, which is why no estimation technique can work. Also, the observed time response and the nominal time response are getting even more similar. At frequency higher than 3 Hz, which are not shown in the time plots, the relative velocities across the suspension start decreasing as the frequency is increased: 3 Hz is close a resonance across the suspensions.

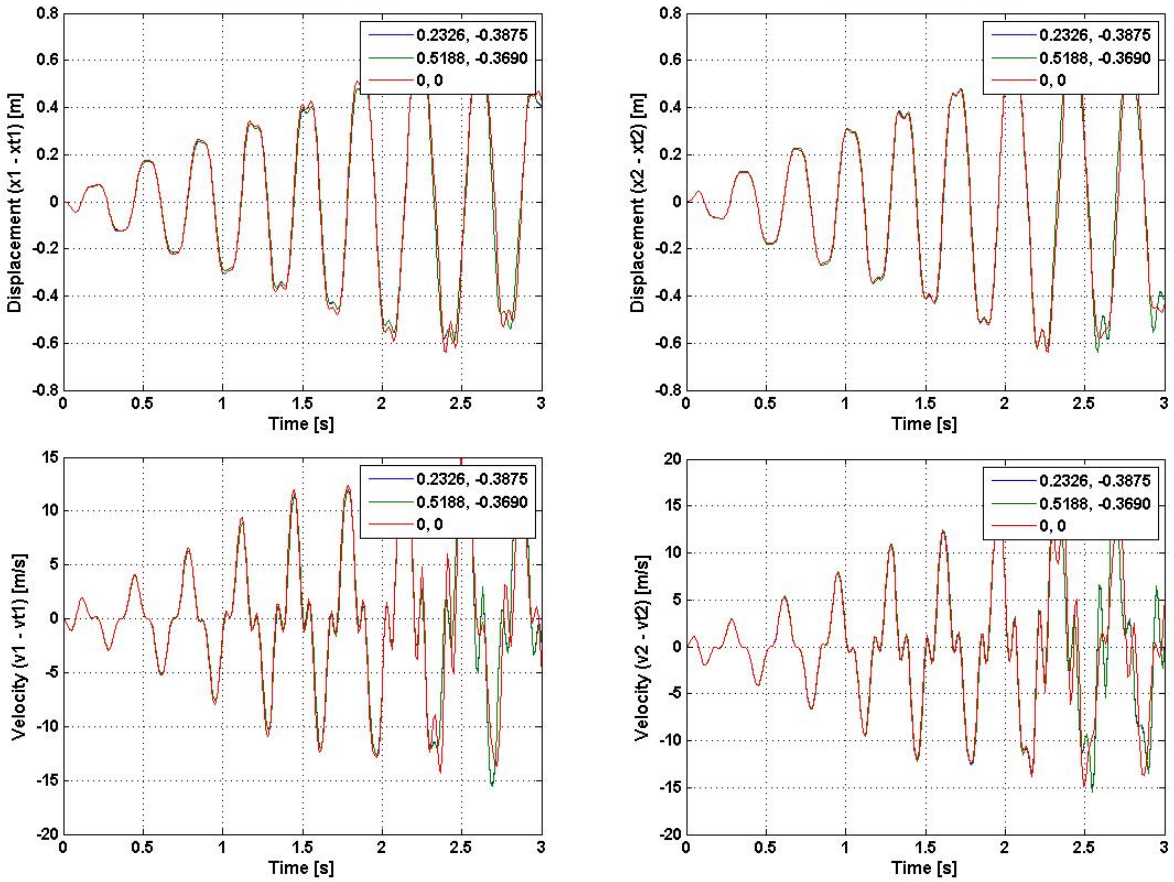

Figure 20. Time Responses at 3 Hz

Let's remind that if *v* is the relative velocity across the damper with a damping coefficient c_i (i = 1, 2), the force across the damper is given by: $F_{C_i}(v) = c_i\left(0.2\tanh(10v)\right)$. The dampers can therefore be considered to be saturating at speeds higher than 0.2 m/s. At high frequency, the velocities get higher and the dampers are in saturation regime more often. When the dampers saturate, different velocities can yield the same force across the damper, which makes the system is non-identifiable at high frequencies.

For a linearized system, i.e., with $F_{C_i}(v) = c_i v$ for the dampers and $k_{i,3} = 0$ for the suspension springs (i = 1, 2), the system become identifiable for all frequencies from 0.33 Hz to 25 Hz, as shown in Figure 21. The estimation is still sensitive to numerical approximations (e.g., in running the ODE's) and the polynomial chaos approximation, which explains why the estimation of the added mass is not always perfect.

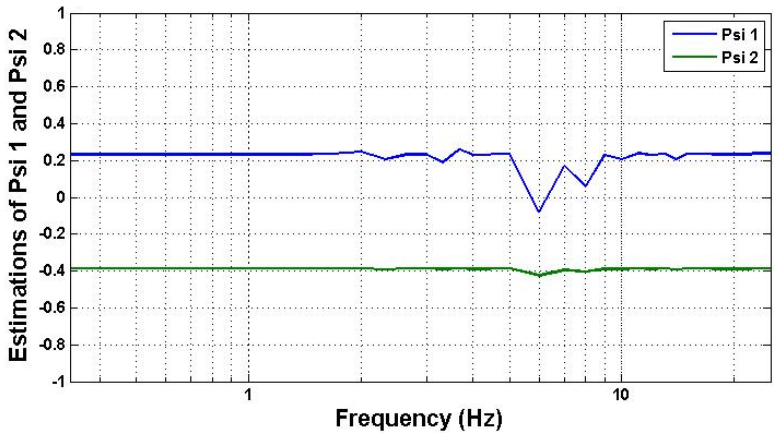

Figure 21. Bayesian Estimation for the Linearized System Using 150 Time Points and a 0.01% Noise

2.6. Regularization

When several combinations of values for the uncertain parameters result in the same behavior of the system, regularization techniques [1] can be used in order to find the most likely values among the values resulting in a minimum, based on our apriori knowledge of the system. It consists of multiplying the apriori part by a coefficient so that the new total cost function has a clear minimum value along the possible values. This is illustrated in Figure 22, where the cost function at 2 Hz is shown for different regularization coefficients.

The cost function will look like its mismatch part when the regularization coefficient is very low and it will look like its apriori part when the regularization coefficient is very high. As the regularization coefficient gets larger, the line of possible minima becomes an ellipse, which starts moving away from the location of the original line of minima while becoming more and more like a circle. Eventually, it becomes a circle centered at (0, 0), like the apriori part of the cost function. When the line becomes an ellipse with a well defined center, the regularization coefficient is large enough and it is not desirable to continue to increase its value since the ellipse will start moving away from its original location while becoming a center. In this case, 10^7 seems to be a good regularization coefficient and it results in the following estimation: $(\xi_1, \xi_2) = (0.05, -0.39)$

When the cost function has a region of possible minimum values that cannot be differentiated, e.g. when dealing with a non-identifiability issue, using regularization techniques will yield better results on average. However, there is no guarantee that it will yield a value closer to the actual values of the uncertain parameters for any given problem. For instance, 2 Hz is not a very relevant example, because the "plain" cost function almost finds the right result. I would need to recomputed everything at a higher frequency where the results is way off, but it will take time

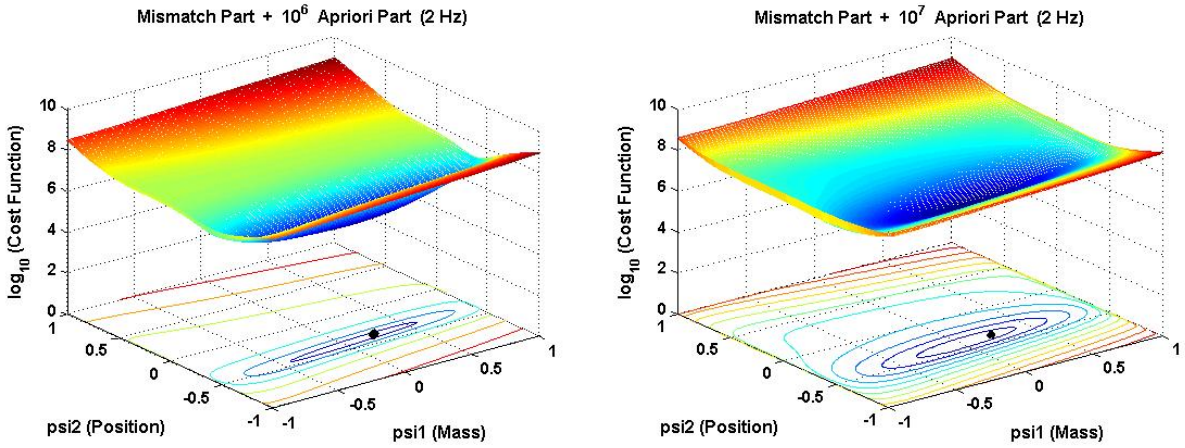

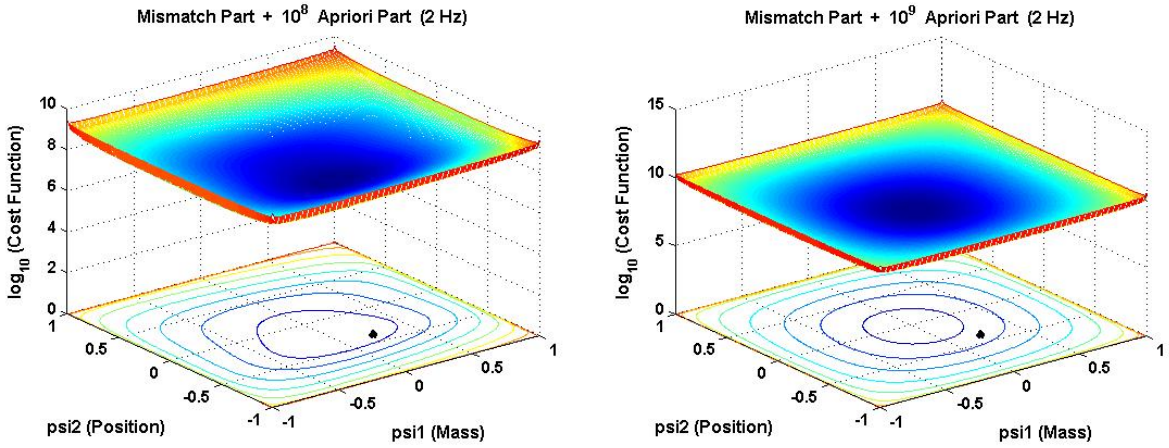

Figure 22. Regularization at 2 Hz

Figure 23 shows the cost function at 3 Hz for different regularization coefficients. In this case, 10^9 seems to be a good regularization coefficient and it results in the following estimation: $(\xi_1, \xi_2) = (0.26, -0.37)$. Regularization techniques are more valuable at 3 Hz than at 2 Hz since the estimation was still working approximately at 2 Hz, but was not accurate at all anymore at 3 Hz for estimating M (i.e. ξ_1).

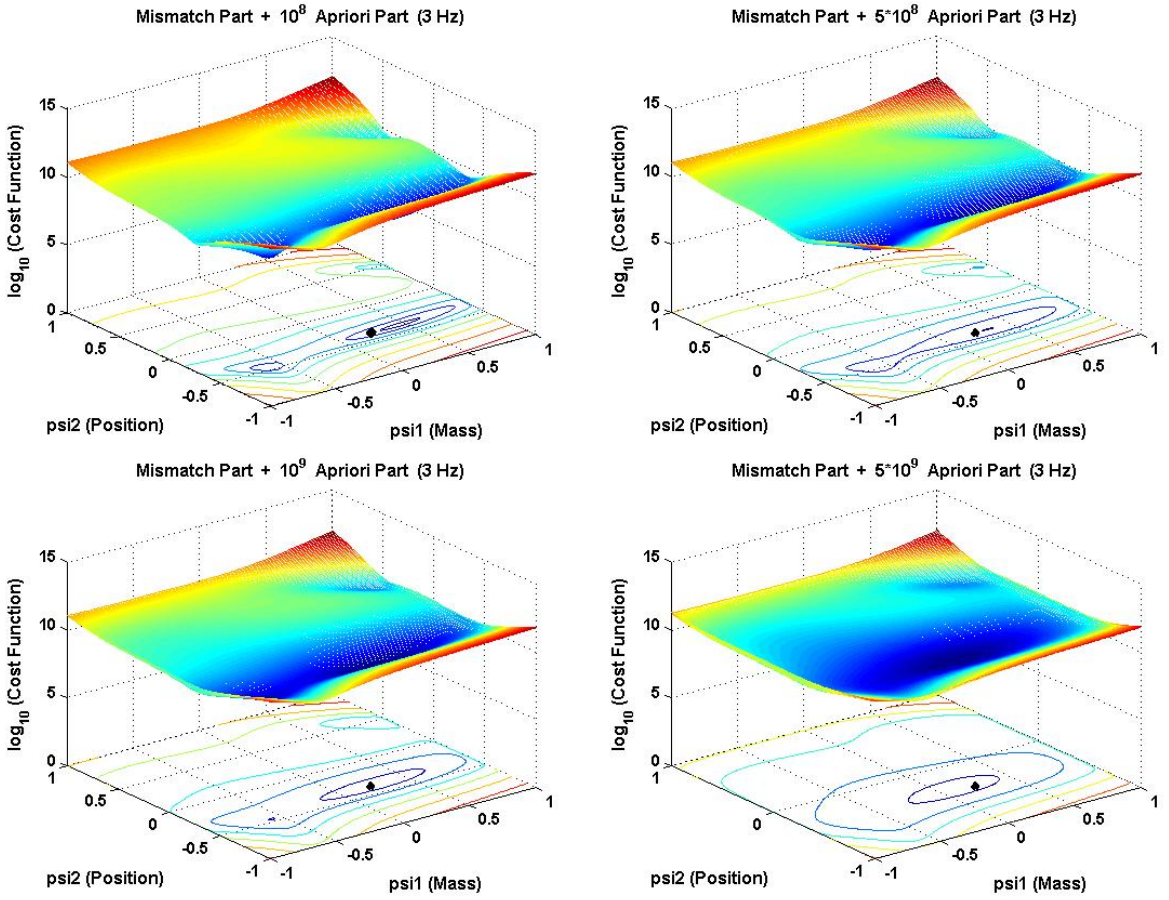

Figure 23. Regularization at 3 Hz

3. SUMMARY AND CONCLUSIONS

The first part of this paper applies the polynomial chaos theory to the problem of parameter estimation, using direct stochastic collocation. The maximum likelihood estimates are obtained by minimizing a cost function derived from the Bayesian theorem. The second part of this paper applies this new computational approach to a mechanical system. Parameter estimation is performed on a nonlinear four degree of freedom roll plane model of a vehicle, in which an uncertain mass with an uncertain position is added on the roll bar. Uncertainties on the values of the added mass and its position are assumed to have a Beta (1, 1) distribution. The value of the mass and its position are estimated from periodic observations of the displacements and velocities across the suspensions. Appropriate excitations are needed in order to obtain accurate results. For some excitations, different combinations of uncertain parameters lead to essentially the same time responses, and no estimation method can work without additional information. Regularization techniques can still yield most likely values among the possible combinations of uncertain parameters resulting in the same time responses than the ones observed. When using appropriate excitations, the results obtained with this approach are close to the actual values of the parameters. The proposed estimation procedure can work with noisy measurements.

The accuracy of the estimations has been shown to be sensitive to the number of terms used in the polynomial expressions and to the number of collocation points, and thus it may become computationally expensive when a very high accuracy of the results is desired. However, the noise level in the measurements affects the accuracy of the estimations as well. Therefore, it is usually not necessary to use a large number of terms in the polynomial expressions and a very large number of collocation points since the addition of extra precision eventually affects the results less than the effect of the measurement noise.

The proposed method has several advantages. Simulations using Polynomial Chaos methods are much faster than Monte Carlo simulations. Another advantage of this method is that it is optimal; it can treat non-Gaussian uncertainties since the Bayesian approach is not tailored to any specific distribution. The cost function can have multiple local minima, which can affect the estimates when dealing with large measurement noise. The proposed estimation procedure can benefit from regularization techniques in order to find a most likely value among these minima based on our apriori knowledge of the system.

Future work will address the estimation problem in the Bayesian framework when both the input excitation and the output signal are reconstructed from. We plan to apply the proposed technique to identify parameters of a real mechanical system for which laboratory measurements are available.

ACKNOWLEDGEMENTS

This research was supported in part by NASA Langley through the Virginia Institute for Performance Engineering and Research award. The authors are grateful to Dr. Mehdi Ahmadian, Dr. Steve Southward, Dr. John Ferris, and Mr. Carvel Holton for many fruitful discussions on this topic.

REFERENCES

[1] Aster , R.C., Borchers, B., and Thurber, C.H.: “Parameter Estimation and Inverse Problems”, Elsevier Academic Press, 2005. ISBN 0-12-065604-3.

[2] Blanchard, E., Sandu, C., and Sandu, A. – “A Polynomial-Chaos-based Bayesian Approach for Estimating Uncertain Parameters of Mechanical Systems”, *Proceedings of the ASME 2007 International Design Engineering Technical Conferences & Computers and Information in Engineering Conference IDETC/CIE 2007, 9th International Conference on Advanced Vehicle and Tire Technologies (AVTT)***,** September 4-7, 2007, Las Vegas, Nevada, USA

[3] Blanchard, E., Sandu, A., and Sandu, C. – “Parameter Estimation Method Using an Extended Kalman Filter”, *Proceedings of the Joint North America, Asia-Pacific ISTVS Conference and Annual Meeting of Japanese Society for Terramechanics*, June 23-26, 2007, Fairbanks, Alaska.

[4] Ghanem, R.G., and Spanos, P.D. – “Stochastic Finite Elements”, Dover Publications Inc, Mineola, New York, 2003.

[5] Ghanem, R.G., and Spanos, P.D. – “Polynomial Chaos in Stochastic Finite Element”, *Journal of Applied Mechanics*, 1990, Vol. 57, 197-202.

[6] Ghanem, R.G., and Spanos, P.D. – "Spectral Stochastic Finite-Element Formulation for Reliability Analysis", *ASCE Journal of Engineering Mechanics*, 1991, Vol. 117, No. 10, 2351-2372.

[7] Ghanem, R.G., and Spanos, P.D. – "A Stochastic Galerkin Expansion for Nonlinear Random Vibration Analysis", Probabilistic Engineering Mechanics, 1993, Vol. 8, No. 3, 255-264.

[8] Halton, J. H., Smith, G. B. "Radical-inverse quasi-random point sequence". *Communications of the ACM*, 7(12):701–702, Dec. 1964.

[9] Hammersley, J. M. "Monte Carlo Methods for Solving Multivariables Problems", *Ann. New York Acad. Sci.*, 86:844–874, 1960.

[10] Li, L., Sandu, C., and Sandu, A. – "Modeling and Simulation of a Full Vehicle with Parametric and External Uncertainties", *Proc. of the 2005 ASME Int. Mechanical Engineering Congress and Exposition, 7th VDC Annual Symposium on "Advanced Vehicle Technologies", Session 4: Advances in Vehicle Systems Modeling and Simulation*, Paper number IMECE2005-82101, Nov. 6-11, 2005, Orlando, FL.

[11] Sandu, A., Sandu, C., and Ahmadian, M. – *Modeling Multibody Dynamic Systems With Uncertainties. Part I: Theoretical and Computational Aspects*, Multibody System Dynamics, Publisher: Springer Netherlands, ISSN: 1384-5640 (Paper) 1573-272X (Online), DOI 10.1007/s11044-006-9007-5, pp. 1-23 (23), June 29, 2006.

[12] Sandu, C., Sandu, A., and Ahmadian, M. – *Modeling Multibody Dynamic Systems With Uncertainties. Part II: Numerical Applications*, Multibody System Dynamics, Publisher: Springer Netherlands, ISSN: 1384-5640 (Paper) 1573-272X (Online), DOI: 10.1007/s11044-006-9008-4, Vol. 15, No. 3, pp. 241 - 262 (22), April 2006.

[13] Sandu, C., Sandu, A., Chan, B.J., and Ahmadian, M. – "Treating Uncertainties in Multibody Dynamic Systems using a Polynomial Chaos Spectral Decomposition", *Proc. of the ASME IMECE 2004, 6th Annual Symposium on "Advanced Vehicle Technology*", Paper number IMECE2004-60482, Nov. 14-19, 2004 Anaheim, CA.

[14] Sandu, C., Sandu, A., Chan, B.J., and Ahmadian, M. – "Treatment of Constrained Multibody Dynamic Systems with Uncertainties", *Proc. of the SAE Congress 2005*, Paper number 2005-01-0936, April 11-14, 2005, Detroit, MI.

[15] Sandu, C., Sandu, A., and Li, L. – "Stochastic Modeling of Terrain Profiles and Soil Parameters", *SAE 2005 Transactions Journal of Commercial Vehicles*, V114-2, 2005-01-3559, 211-220, Feb, 2006.

[16] Simon, D. E. "An Investigation of the Effectiveness of Skyhook Suspensions for Controlling Roll Dynamics of Sport Utility Vehicles Using Magneto-Rheological Dampers", Ph.D. Thesis, Virginia Tech, Blacksburg, VA, 24061, 2001.

[17] Sohns, B., Allison, J., Fathy, H. K., Stein, J. L. "Efficient Parameterization of Large-Scale Dynamic Models Through the Use of Activity Analysis", *Proceedings of the ASME IMECE 2006*, IMECE2006, Nov 5-10, 2006, Chicago, Illinois.

[18] Xiu, D., Lucor, D., Su, C.-H., and Karniadakis, G.E. – "Stochastic Modeling of Flow-Structure Interactions using Generalized Polynomial Chaos", *J. Fluids Engineering*, Vol. 124, 51-59, 2002.

[19] Xiu, D., and Karniadakis, G. E. – "The Wiener-Askey Polynomial Chaos for Stochastic Differential Equations", *Journal of Sci Comput*, 2002: Vol. 24, No. 2: 619-644.

[20] Xiu, D., and Karniadakis, G.E. – "Modeling Uncertainty in Flow Simulations via Generalized Polynomial Chaos", *Journal of Computational Physics*, 2003: Vol. 187: 137-167.

[21] Xiu, D., and Karniadakis, G.E. – "Modeling Uncertainty in Steady-state Diffusion problems via Generalized Polynomial Chaos", Computer Methods in Applied Mechanics and Engineering, 2002: Vol. 191: 4927-4928.

[22] Zhang, D., Lu., Z. "An efficient, high-order perturbation approach for flow in random porous media via Karhunen–Loeve and polynomial expansions", *J Comp. Phys.* 54:265–291 (2006)

LIST OF FIGURES

LIST OF TABLES